PROCEEDINGS of the
23rd International Congress on Acoustics
9 to 13 September 2019 in Aachen, Germany

Noise from a blunt edged flat plate in a reverberant water tunnel

Paul CROAKER[(1)], James VENNING[(2)], Mahmoud KARIMI[(3)], Paul BRANDNER[(2)], Con DOOLAN[(1)], Nicole KESSISSOGLOU[(1)]

[(1)]School of Mechanical & Manufacturing Engineering, UNSW, Sydney, Australia
[(2)]Cavitation Research Laboratory, University of Tasmania, Launceston, Australia
[(3)]Centre for Audio, Acoustics and Vibration, University of Technology Sydney, Sydney, Australia

Abstract

An experimental and numerical investigation of the flow around and noise produced by a blunt edged flat plate in a reverberant water tunnel is presented. The flow is at a Reynolds number based on chord of 6.8×10^6 and a Mach number of 5.3×10^{-3}. Experimental measurements were taken in the Australian Maritime College Cavitation Research Laboratory closed recirculating variable-pressure water tunnel. Hydrophones mounted in the tunnel wall and pressure sensors attached to the plate were used to measure the pressures generated by the turbulent flow over the plate. A large eddy simulation was also conducted, with hydrodynamic pressures on the surface of the plate extracted and combined with Curle's acoustic analogy to predict the pressure fluctuations on the wall of the water tunnel. The numerical predictions are found to agree well with the experimental measurements.

Keywords: Flow-induced noise, Computational hydroacoustics, Experimental measurement

1 INTRODUCTION

The aim of the present work is to investigate and measure non-cavitating flow-induced noise within the Australian Maritime College Cavitation Research Laboratory closed recirculating variable-pressure water tunnel and to numerically predict this noise. Development and application of flow-induced noise prediction techniques have focused almost exclusively on aerodynamically generated sound, see for example Refs. [1, 2, 3, 4]. Further, a large number of high quality aeroacoustic flow and noise measurements are present in the literature [5, 6, 7, 8]. These studies provide a valuable source of benchmark data for development of predictive numerical models.

Applying aeroacoustic prediction techniques to study the generation and propagation of flow-induced noise in water is not always straight forward. This was demonstrated in the recent work of Ianniello [9]. He showed that non-linear flow noise sources, traditionally neglected in low Mach number aeroacoustics, make a significant contribution to the flow-induced noise generated by a marine propeller. Also, marine applications are characterised by very high Reynolds numbers and very low Mach numbers which further widens the separation of hydrodynamic and acoustic scales that are present in aeroacoustic problems. It is therefore important to develop numerical flow-induced noise prediction techniques for hydroacoustic applications and to validate these techniques against experimental measurements of flow noise obtained in water.

In the present work, experiments on the flow and noise produced by a blunt edged flat plate are conducted in the Australian Maritime College Cavitation Research Laboratory closed recirculating variable-pressure water tunnel. A large eddy simulation (LES) analysis of the flow is also conducted with the surface pressure on the plate extracted and combined with a modified version of Curle's analogy to account for the reflection of pressure waves off the walls of the water tunnel. Numerical results and measured data are compared and discussed.

2 EXPERIMENTAL SETUP

All experiments were carried out in the Australian Maritime College Cavitation Research Laboratory closed recirculating variable-pressure water tunnel. A schematic diagram of the tunnel circuit is shown in Figure 1.

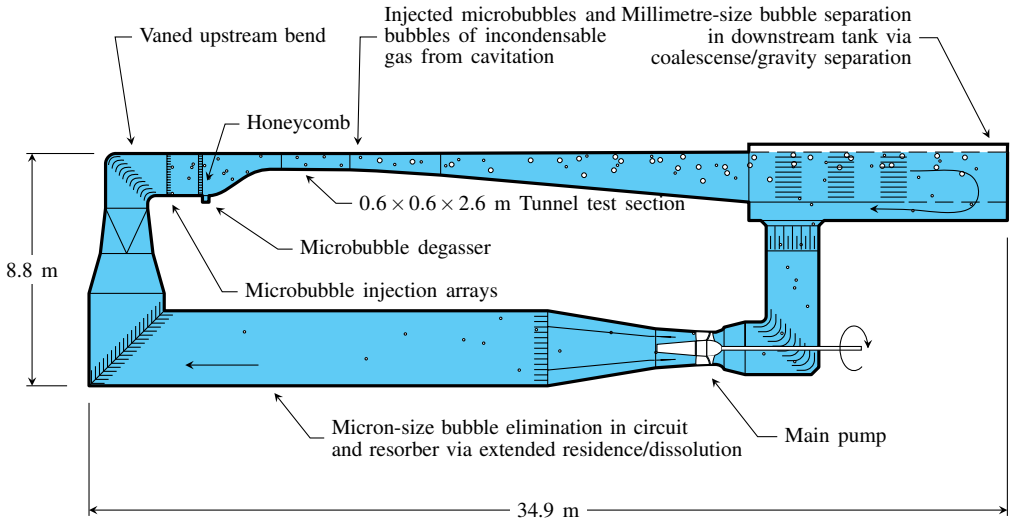

Figure 1. Schematic diagram of the variable-pressure water tunnel showing circuit architecture for continuous removal of microbubbles or large volumes of injected incondensable gas and ancillaries for microbubble seeding and for degassing of water. Microbubbles may be either injected for modelling cavitation nucleation or generated by the cavitation itself.

The tunnel test section is 0.6 m square by 2.6 m long and the tunnel volume is 365 m^3 with demineralised water the working fluid. The nominal operating velocity and absolute-pressure ranges are 2 to 13 m/s and 4 to 400 kPa, respectively. The circuit has low background noise and vibration levels due to low velocities and isolation from the surrounding building and all noise-generating machinery. The cavitation tunnel design and specification is described in detail in [10].

A stainless steel rectangular plate with elliptical (4:1) leading edge was mounted vertically at the mid-span of the tunnel test section as shown in Figure 2. The thickness H, is 46 mm and chord, L is 850 mm, giving a test section blockage of 7.7%. The freestream velocity was maintained at 7.93 m/s such that the chord-based Reynolds number was 6.8×10^6 and the Mach number was 5.3×10^{-3}. The freestream absolute pressure was maintained at 105 kPa and no cavitation was observed.

The hydrodynamic noise was measured with two hydrophones and three pressure sensors. The hydrophones were Brüel and Kjær type 8103 models with a frequency range up to 180 kHz. One hydrophone was mounted in the tunnel wall 70 mm downstream of the trailing edge of the plate. The wall-mounted hydrophone was installed in a flooded cavity behind a 149 mm diameter, 10 mm thick polyurethane diaphragm as described in [11]. The acoustic impedance of polyurethane is nearly the same as water, providing a near reflection-free acoustic interface. The large sensing area of the diaphragm provides attenuation of the boundary layer turbulent noise. The in-flow hydrophone was positioned 150 mm away from the tunnel wall and 280 mm downstream of the trailing edge of the plate. Both these hydrophone signals were conditioned with a Brüel and Kjær type 2692 charge amplifier with a 0.1 Hz low-pass filter and a 100 kHz high-pass filter. Signals were recorded for 81 s with an acquisition rate of 204.8 kHz. Only results for the wall-mounted hydrophone are presented here.

The three pressure sensors were quartz-type PCB 105C02 sensors with 2.5 mm diameter sensing surfaces and a resonant frequency of at least 250 kHz. Two pressure sensors were mounted in the two sides of the plate, 23 mm upstream of the trailing edge. These are labelled ‘near’ and ‘far’ and are situated 311.5 mm and 288.5 mm from the tunnel ceiling respectively. The third pressure sensor is located in the rear surface of the plate, 300 mm from the ceiling. These signals were conditioned with a Kistler 5080A amplifier.

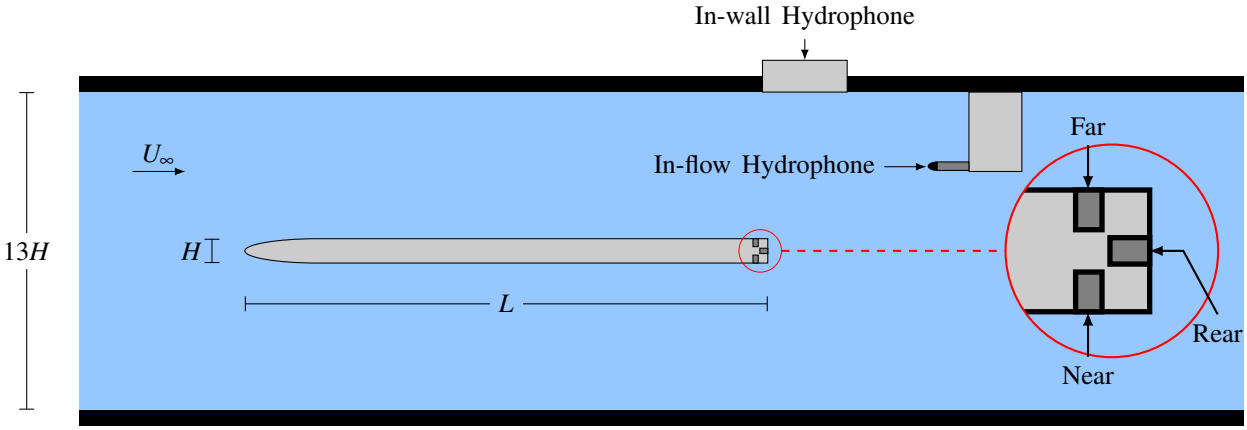

Figure 2. Top-view of the bluff plate as it is placed in the tunnel test-section.

3 NUMERICAL FLOW-INDUCED NOISE PREDICTION

3.1 Hydrodynamic Data and Acoustic Sources

In addition to the experiments, an LES of the unsteady flow field around the plate is performed by filtering the incompressible Navier-Stokes equations to separate the hydrodynamic fluctuations into resolved and sub-grid scale components. The filtered incompressible Navier-Stokes equations are given by

$$\rho_f \frac{\partial \hat{u}_i}{\partial t} + \rho_f \frac{\partial}{\partial y_i}\left(\hat{u}_i \hat{u}_j\right) = -\frac{\partial \hat{p}}{\partial y_j} + 2\left(\mu_f + \mu_{\mathrm{SGS}}\right)\frac{\partial}{\partial y_j}\hat{S}_{ij} \tag{1}$$

$$\frac{\partial \hat{u}_j}{\partial y_j} = 0 \tag{2}$$

where $\hat{p}$ is the filtered pressure and $\hat{u}_i$ represents components of the resolved velocity vector. μ_f and ρ_f are the viscosity and density of the fluid at rest. $\hat{S}_{ij}$ is the strain rate tensor of the resolved scales. The wall-adapting local eddy-viscosity model in [12] is used to define the eddy viscosity, μ_{SGS}, which accounts for the influence of the sub-grid scales on the filtered motion. Due to the high Reynolds number, it is computationally impractical to resolve the velocities into the plate viscous sublayer. Instead, the wall model of Spalding [13] is used to model the effect of the near wall stresses on the flow.

A hybrid mesh is constructed comprising a fully structured core mesh around the plate and in the wake region, as well as an unstructured mesh created away from the plate to reduce cell count. Further, only a 0.07 m spanwise section of the model has been considered with periodic boundary conditions applied to reduce the total number of CFD cells. The flat plate CFD model contained a total of 110×10^6 hexahedral cells. The streamwise, wall normal and spanwise near wall cell sizes in non-dimensional wall units are $x^+ \approx 50$, $y^+ \approx 12$ and $z^+ \approx 60$, respectively. The CFD model extends 1.5 m upstream of the leading edge and 3.65 m downstream of the trailing edge. Figure 3 shows the CFD model and associated mesh.

The pressure implicit with splitting of operator (PISO) algorithm was used to deal with the pressure-velocity coupling during solution of the LES equations. A second-order backward implicit scheme was utilised for the temporal discretisation. A blended spatial differencing scheme was used with 80% second order central differencing and 20% second order upwind differencing for the non-linear terms in the momentum equations. A standard second order central differencing scheme was applied for all other spatial discretisations.

The transient simulation was executed with a time step size of 2.5×10^{-6} s and was allowed to progress until

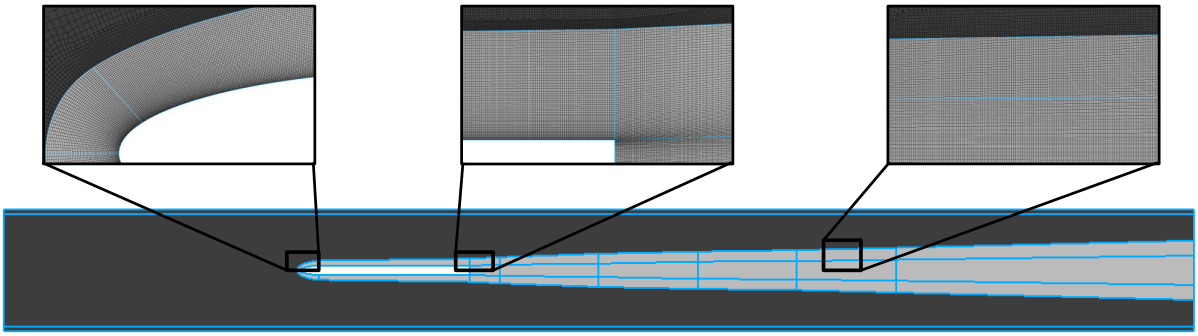

Figure 3. CFD model for the blunt edge flat plate, inserts show the CFD mesh near the leading and trailing edges and the far wake.

the flow field achieved quasi-periodicity. Recording of the surface pressures on the plate then commenced with the pressure stored at intervals of 5×10^{-4} s. Curle [14] demonstrated that at low Mach numbers, the dominant contribution to the sound produced by a body in flow can be represented by a distribution of dipoles on the surface of the body, with the dipole force obtained from the surface pressure. Time histories of the surface pressures were divided into equal segments with a length of 458 records and 50% overlap. A Hanning window function was applied to each segment of the surface pressure time histories before converting them to frequency spectra.

3.2 Propagation of Flow-Induced Pressure Waves

The pressure waves generated by fluctuating surface pressures propagate to the far field and are reflected, scattered and diffracted by objects in their path. This is of particular importance in the reverberant environment of the water tunnel. To account for reflection of the pressure waves by the tunnel walls, the method of images is used to consider multiple radiation paths from surface sources to the receiver location. Based on Curle's analogy, the pressure at a receiver point is given by [14]

$$p_a(\mathbf{x},\omega) = \int_S p(\mathbf{y},\omega) \frac{\partial G_r(\mathbf{x},\mathbf{y},\omega)}{\partial n} dS \tag{3}$$

where $\mathbf{x}$ is the location at which the pressure is computed. S is the surface of the plate, $\mathbf{y}$ is a source point on the plate and n is the unit normal at the source point. p is the surface pressure and ω is the angular frequency. $G_r(\mathbf{x},\mathbf{y},\omega)$ is the three-dimensional harmonic Green's function used to describe the propagation of the acoustic waves from source point $\mathbf{y}$ to receiver point $\mathbf{x}$ and includes the influence of the image receivers as follows

$$G_r = \sum_{s=0}^{N} \frac{e^{ik_a|\mathbf{x}_s-\mathbf{y}|}}{4\pi|\mathbf{x}_s-\mathbf{y}|} \tag{4}$$

where $i = \sqrt{-1}$, k_a is the acoustic wave number and $\mathbf{x}_s$ is the location of the s^{th} image receiver. s=0 represents the physical receiver location. In the present work, 10 image receivers were used for each of the top, bottom, left and right walls of the tunnel, representing a total of 41 receivers including the physical receiver location.

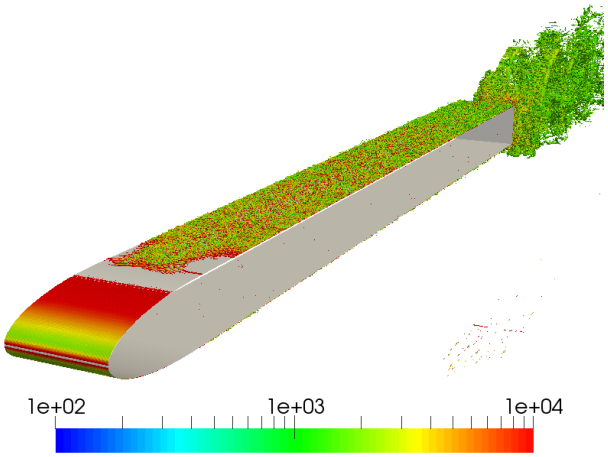

Figure 4. Isosurfaces of Q-criteria coloured by vorticity magnitude.

4 RESULTS AND DISCUSSION

4.1 Hydrodynamic flow field

Figure 4 presents isosurfaces of the Q-criterion coloured by the magnitude of the vorticity vector and shows the structures in the flow past the plate. Slightly downstream of the elliptical leading edge, the flow undergoes laminar to turbulence transition with the turbulent boundary layer developing along the length of the plate. At the blunt trailing edge the flow separates, forming two shear layers which roll up into vortices that are shed into the wake forming a von Karman vortex street. Figure 4 shows that the vortices contain flow features with a wide range of scales. Hence the pressure waves produced at the vortex shedding frequency and its harmonics are likely to contain significant broadening of the tonal peaks. Also, the smaller scale turbulent structures in the boundary layer that convect past the blunt trailing edge are expected to produce broadband noise at higher frequencies.

4.2 Surface pressure results and measurements

Figure 5 presents a comparison between the measured and predicted surface pressure at the 'near' pressure sensor location shown in Figure 2. The broadened tonal peaks correspond to the vortex shedding frequency and its harmonics. The LES simulation predicts the vortex shedding frequency to occur at a non-dimensional Strouhal number based on thickness of St_h=0.252 which is within 7% of the measured value of 0.236. Within the frequency range from 10 Hz to 400 Hz, the autospectral density of the trailing edge pressure predicted with the LES follows the same general shape observed in the measured data, with the vortex shedding frequency and its second and third harmonics well captured. However, the magnitude of the autospectral density of the trailing edge pressure predicted by the LES within this frequency range is between 3 to 6 dB higher than the measured value. It is important to note that the same frequency bandwidth was used for both numerical and experimental data processing to ensure that the tonal peaks from both data sets encounter the same averaging. Above this frequency range the predicted surface pressure diverges from the measured data. Additional LES analyses are currently being carried out in an attempt to improve the agreement between predicted and measured surface pressure data.

4.3 Wall mounted hydrophone results and measurements

The surface pressures on the plate, predicted with the LES analysis, are combined with Curle's analogy using equation (3) and including 40 image receivers to account for reflections off the tunnel walls. The pressure at the

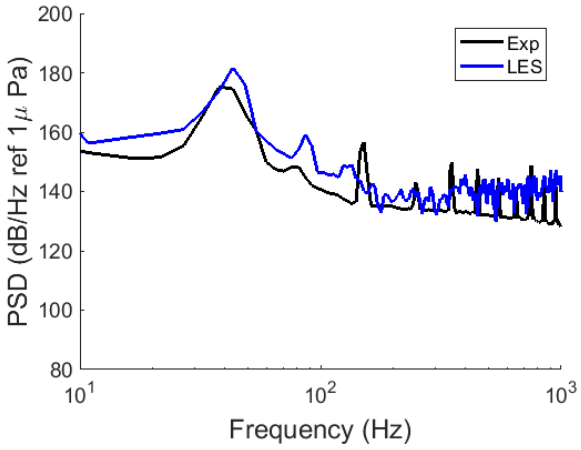

Figure 5. Autospectral density of the surface pressure at the trailing edge.

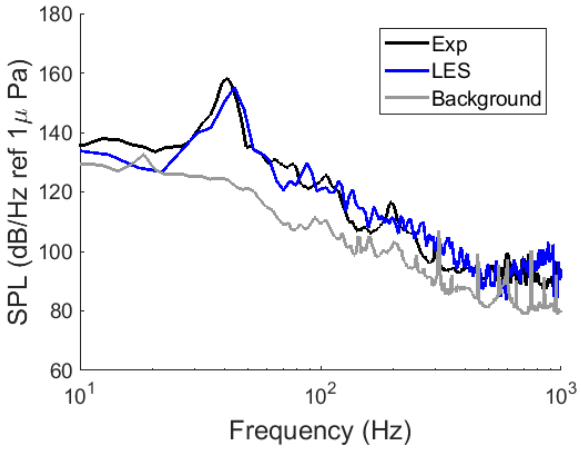

Figure 6. Comparison of predicted and measured pressure at the wall mounted hydrophone location.

wall mounted hydrophone location is then estimated. Figure 6 shows that there is excellent agreement between the sound pressure level (SPL) predicted from the LES/acoustic analogy approach and the measured pressure at the wall mounted hydrophone. The broadened tonal peak at the vortex shedding frequency is well predicted as is the broadband pressure at higher frequencies. However, the ongoing LES analyses that aim to achieve greater agreement between predicted and measured surface pressures near the trailing edge of the plate may change the predicted wall mounted hydrophone pressures and this will be assessed in the future work. Figure 6 also shows the background noise level measured for 8 m/s flow in the tunnel with no plate present. There is sufficient difference between background noise levels and the pressure levels measured at the wall mounted hydrophone when the plate is present to allow for meaningful comparison between numerical and measured data.

5 CONCLUSIONS

Experimental measurements and numerical predictions of the flow and noise produced by a blunt edged flat plate in a reverberant water tunnel has been presented. The experimental data indicates that the flow-induced

noise levels measured at the wall mounted hydrophone are significantly above the background noise levels of the tunnel and hence are suitable for validation of numerical predictions of the flow-induced noise. The large eddy simulation of the flat plate, and subsequent prediction of the pressure fluctuations at the wall mounted hydrophone location using an acoustic analogy agree well with the measured data.

References

[1] Seo JH, Moon YJ. Aerodynamic noise prediction for long-span bodies. Journal of Sound and Vibration. 2007;306:564–579.

[2] Wang M, Moreau S, Iaccarino G, Roger M. LES prediction of wall-pressure fluctuations and noise of a low-speed airfoil. International Journal of Aeroacoustics. 2009;8:177–198.

[3] Wolf WR, Lele SK. Acoustic analogy formulations accelerated by fast multipole method for two-dimensional aeroacoustic problems. AIAA Journal. 2010;48:2274–2285.

[4] Croaker P, Kessissoglou N, Marburg S. Aeroacoustic scattering using a particle accelerated computational fluid dynamics/boundary element technique. AIAA Journal. 2016;54(7):2116–2133.

[5] Jacob MC, Boudet D, Casalino D, Michard M. A rod-airfoil experiment as a benchmark for broadband noise modelling. Theoretical and Computational Fluid Dynamics. 2005;19:171–196.

[6] Devenport WJ, Staubs JK, Glegg SAL. Sound radiation from real airfoils in turbulence. Journal of Sound and Vibration. 2010;329:3470–3483.

[7] Moreau D, Brooks L, Doolan C. The effect of boundary layer type on trailing edge noise from sharp-edged flat plates at low-to-moderate Reynolds number. Journal of Sound and Vibration. 2012;331:3976–3988.

[8] Moreau DJ, Doolan CJ, Alexander WN, Meyers TW, Devenport WJ. Wall-mounted finite airfoil-noise production and prediction. AIAA Journal. 2016;54(5):1637–1651.

[9] Ianniello S. The Ffowcs Williams-Hawkings equation for hydroacoustic analysis of rotating blades. Part 1. The rotpole. Journal of Fluid Mechanics. 2016;797:345–388.

[10] Brandner PA, Lecoffre Y, Walker GJ. Design considerations in the development of a modern cavitation tunnel. In: Proceedings of the 16th Australasian Fluid Mechanics Conference. Crown Plaza, Gold Coast, Australia; 2007. .

[11] Doolan C, Brandner P, Butler D, Pearce B, Moreau D, Brooks L. Hydroacoustic characterisation of the AMC cavitation tunnel. In: Acoustics 2013 - Victor Harbor. Victor Harbor, Australia; 2013. .

[12] Nicoud F, Ducros F. Subgrid-scale stress modelling based on the square of the velocity gradient tensor. Flow, Turbulence and Combustion. 1999;62(3):183–200.

[13] Spalding DB. A single formula for the "law of the wall". Journal of Applied Mechanics. 1961;28:455–458.

[14] Curle N. The influence of solid boundaries upon aerodynamic sound. Proceedings of the Royal Society of London Series A, Mathematical and Physical Sciences. 1955;231:505–514.